

Two-photon and three-photon blockades in driven nonlinear systemsAdam Miranowicz,^{1,2} Małgorzata Paprzycka,¹ Yu-xi Liu,^{2,3,4} Jiří Bajer,⁵ and Franco Nori^{2,6}¹*Faculty of Physics, Adam Mickiewicz University, PL-61-614 Poznań, Poland*²*Advanced Science Institute, RIKEN, Wako-shi, Saitama 351-0198, Japan*³*Institute of Microelectronics, Tsinghua University, Beijing 100084, China*⁴*Tsinghua National Laboratory for Information Science and Technology (TNList), Tsinghua University, Beijing 100084, China*⁵*Department of Optics, Palacký University, 772 00 Olomouc, Czech Republic*⁶*Physics Department, The University of Michigan, Ann Arbor, Michigan 48109-1040, USA*

(Received 18 December 2012; published 8 February 2013)

Photon blockade, in analogy to Coulomb's or phonon blockades, is a phenomenon when a single photon in a nonlinear cavity blocks the transmission of a second photon. This effect can occur in Kerr-type systems driven by a laser due to strong nonlinear photon-photon interactions. We predict the occurrence of higher-order photon blockades where the transmission of more than two photons is effectively blocked by single- and two-photon states. This photon blockade can be achieved by tuning the frequency of the laser driving field to be equal to the sum of the Kerr nonlinearity and the cavity resonance frequency. We refer to this phenomenon as two-photon blockade or two-photon state truncation via nonlinear scissors, and can also be interpreted as photon-induced tunneling. We also show that, for a driving-field frequency fulfilling another resonance condition and for higher strengths of the driving field, even a three-photon blockade can occur but less clearly than in the case of single- and two-photon blockades. We demonstrate how various photon blockades can be identified by analyzing photon-number correlations, coherence and entropic properties, Wigner functions, and spectra of squeezing. We show that two- and three-photon blockades can, in principle, be observed in various cavity and circuit quantum electrodynamical systems for which the standard single-photon blockade was observed without the need of using higher-order driving interactions or Kerr media exhibiting higher-order nonlinear susceptibility.

DOI: [10.1103/PhysRevA.87.023809](https://doi.org/10.1103/PhysRevA.87.023809)

PACS number(s): 42.65.Hw, 42.50.Lc

I. INTRODUCTION

In nonlinear optical systems driven by a coherent classical light in a cavity, a single photon can impede the transmission of other photons. This phenomenon is referred to as *photon blockade* (PB) [1], in close analogy to the phenomenon of *Coulomb's blockade* [2], where electron transport is blocked by a strong Coulomb interaction in a confined structure. In PB the next photon can enter the cavity only if the first photon has left it; thus, a sequence of single photons can be generated and such system can act as a single-photon turnstile device. Evidently, the PB changes classical light into highly nonclassical light exhibiting, in particular, photon antibunching and sub-Poisson photon-number statistics.

The PB can be interpreted as nonlinear *optical-state truncation* or *nonlinear quantum scissors* [3,4], since the infinitely dimensional Fock-state expansion of a classical driving field is truncated at the single-photon Fock's state. The required nonlinearity can be induced by a strong interaction between the cavity and the two-level (natural or artificial) atom.

The PB has been predicted in various setups in cavity quantum electrodynamics (QED) [5–11], and recently also in circuit QED [12,13]. The PB was first demonstrated experimentally with a single atom trapped in an optical cavity [14]. This experiment was considered “a landmark event in the field of quantum optics and laser science” [15]. In solid-state systems, the PB was experimentally demonstrated with a quantum dot in a photonic crystal cavity [16] and with a single superconducting artificial atom coupled to a microwave transmission-line resonator (superconducting “cavity”) [12,13]. The PB was also predicted in quantum optomechanical systems [17].

An analogous phenomenon of *phonon blockade* was predicted for an artificial superconducting atom coupled to a nanomechanical resonator [18]. The phonon blockade can be detected via the PB if this system is additionally coupled with, e.g., a superconducting microwave cavity [19].

The PB can have applications in quantum state engineering for the controllable generation of a train of single photons exhibiting highly nonclassical photon statistics. This suggests that the PB (together with phonon blockades) can also be used as an indicator of nonclassicality of mechanical systems [18,19]. As another example of quantum engineering, the PB was also studied in the context of cavity electromagnetically induced transparency in, e.g., Refs. [6,9]. The possibility of tunable (by a classical driving field) transmission from photon blockade to photon transparency in circuit-QED systems was described in Ref. [20].

Moreover, single-photon tunneling, in close analogy to single-electron tunneling, was experimentally observed during light transmission through individual subwavelength pinholes [11]. This effect was explained in terms of the PB, analogously to the Coulomb blockade demonstrated in single-electron tunneling. A close analogy between the PB and Coulomb blockade was also analyzed in Ref. [20] by presenting, e.g., a photonic analog of the Coulomb staircase. Such studies shed more light on quantum simulations of condensed-matter phenomena via optical effects and vice versa.

In this paper, we show the possibility of observing the multiphoton blockade in the standard cavity QED and circuit QED systems, where the single-photon blockade was already observed. These systems consist of a Kerr nonlinearity in a

cavity driven by a classical weak field. We will show how to change the intensity and frequency of the driving field for a given cavity frequency and the Kerr nonlinearity in order to observe the two- and three-PBs.

Those multi-PBs can also be explained as *photon-induced tunneling*. That is, when there is a photon inside the cavity, then the second or third photon can be absorbed by the cavity via two-photon or three-photon processes.

Effects leading to multi-PB were already studied in the literature as generalizations of the single-PB. For example, several systems based on higher-order parametric driving processes and/or higher-order Kerr nonlinearity were analyzed in Refs. [21–23] for the observation of the nonstationary-field multi-PB. In the Conclusions, we will briefly discuss the formal differences and crucial experimental advantages of our approach over these methods.

There is another approach to the PB, which is based on linear systems, while the nonlinearity is induced by measurements. This method is usually referred to as the linear optical state truncation or linear scissors [24]. The multiphoton state truncations (or multi-PBs) implemented via linear scissors were studied in Refs. [25,26], as a generalization of the single-photon state truncation [24,27]. It is worth stressing that the PBs studied in this paper are based on completely different principles and resources. We use, as in the original single-PB proposals [1,3], nonlinear systems (which cause nonlinear photon-photon interactions) without measurements. Thus, the method used here can be referred to as nonlinear scissors [4].

The paper is organized as follows. In Sec. II, we explain the occurrence of the single-PB and describe the method to observe blockades up to two and three photons. In Sec. III, we demonstrate analytically the occurrence of the two-PB in comparison to the single-PB. In Sec. IV, we discuss various signatures of the two-PB revealed by the photon-number statistics, entropies, Wigner functions, and spectra of squeezing. We summarize our main results in the concluding section.

II. FROM SINGLE-PHOTON TO MULTIPHOTON BLOCKADES

A. Hamiltonians

Photon-blockade effects can be observed in a cavity with a nonlinear medium coherently driven by a laser field as described by the following effective Hamiltonian [1,3]:

$$\hat{H} = \hbar\omega_0\hat{a}^\dagger\hat{a} + \hbar\chi(\hat{a}^\dagger)^2\hat{a}^2 + \hbar\epsilon(\hat{a}e^{i\omega_d t} + \hat{a}^\dagger e^{-i\omega_d t}), \quad (1)$$

where \hat{a} (\hat{a}^\dagger) denotes the annihilation (creation) operator, ω_0 is the resonance frequency of the cavity, ω_d is the driving laser frequency, $\chi > 0$ is the Kerr nonlinearity, i.e., the photon-photon interaction strength proportional to the real part of the third-order nonlinear susceptibility $\text{Re}(\chi^{(3)})$, and $\epsilon > 0$ is the driving strength (the Rabi frequency of the laser).

Equation (1) presents an effective Hamiltonian, which can be obtained from various microscopic Hamiltonians describing a variety of systems. For example, one can analyze a quantum two-level system (qubit) off-resonantly coupled to a driven cavity. This system can be described in the rotating-wave

approximation by the following Hamiltonian:

$$\hat{H} = \frac{1}{2}\hbar\omega\hat{\sigma}_z + \hbar\omega'_0\hat{a}^\dagger\hat{a} + \hbar g(\hat{\sigma}^+\hat{a} + \hat{a}^\dagger\hat{\sigma}^-) + \hbar\epsilon(\hat{a}e^{i\omega_d t} + \hat{a}^\dagger e^{-i\omega_d t}), \quad (2)$$

where the first three terms correspond to the standard Jaynes-Cummings Hamiltonian and the last term, as in Eq. (1), describes the interaction between the quantum cavity mode and the classical driving field with strength ϵ . Moreover, $\sigma_z = |e\rangle\langle e| - |g\rangle\langle g|$ denotes the Pauli operator, $\sigma^+ = |e\rangle\langle g|$ ($\sigma^- = |g\rangle\langle e|$) is the qubit raising (lowering) operator, $|g\rangle$ ($|e\rangle$) is the ground (excited) state of the qubit, ω is the qubit transition frequency, and ω'_0 is the resonance frequency of the cavity in Eq. (2). Moreover, other quantities are explained below Eq. (1). This Hamiltonian in the dispersive approximation, where the qubit remains in its ground state, can be reduced to the Hamiltonian, given by Eq. (1) (for a derivation see, e.g., Refs. [18,28] in the circuit QED context).

The unitary operation $\hat{U} = \exp(-i\omega_d\hat{a}^\dagger\hat{a}t)$ transforms the Hamiltonian (1) into

$$\hat{H}_{\text{rot}} = \hat{U}^\dagger\hat{H}\hat{U} - i\hbar\hat{U}^\dagger\frac{\partial}{\partial t}\hat{U}. \quad (3)$$

Thus, in the rotating frame, one obtains the following time-independent Hamiltonian:

$$\hat{H}_{\text{rot}}^{(1)} = \hbar\Delta_1\hat{a}^\dagger\hat{a} + \hbar\chi(\hat{a}^\dagger)^2\hat{a}^2 + \hbar\epsilon(\hat{a} + \hat{a}^\dagger), \quad (4)$$

where $\Delta_1 = \omega_0 - \omega_d$. The single-PB can be observed in the resonant case $\omega_d = \omega_0$ assuming that the driving strength ϵ is much smaller than the Kerr nonlinearity χ . This effect can be interpreted as the single-photon Fock state blockading the generation of two or more photons.

We observe that Hamiltonian (4) can be rewritten as follows:

$$\hat{H}_{\text{rot}}^{(k)}(\Delta_k) = \hbar\Delta_k\hat{a}^\dagger\hat{a} + \hbar\chi\hat{a}^\dagger\hat{a}(\hat{a}^\dagger\hat{a} - k) + \hbar\epsilon(\hat{a} + \hat{a}^\dagger), \quad (5)$$

where the frequency mismatch is

$$\Delta_k = \omega_0 + \chi(k - 1) - \omega_d \quad (6)$$

for some positive k . For convenience, we shall refer to k as a tuning parameter. In the special case of $k = 1$, this Hamiltonian reduces to the standard form, given by Eq. (4).

B. Steady states as a function of the tuning parameter k

The evolution of the system, given by Eq. (5), for the reduced density operator $\hat{\rho}(t)$ under Markov's approximation, can be governed by the standard master equation [29], which for the steady state $\hat{\rho}_{\text{ss}} = \hat{\rho}(t \rightarrow \infty)$ is given by

$$0 = -\frac{i}{\hbar}[\hat{H}_{\text{rot}}^{(k)}(\Delta_k), \hat{\rho}_{\text{ss}}] + \frac{\gamma}{2}\bar{n}_{\text{th}}(2\hat{a}^\dagger\hat{\rho}_{\text{ss}}\hat{a} - \hat{a}\hat{a}^\dagger\hat{\rho}_{\text{ss}} - \hat{\rho}_{\text{ss}}\hat{a}\hat{a}^\dagger) + \frac{\gamma}{2}(\bar{n}_{\text{th}} + 1)(2\hat{a}\hat{\rho}_{\text{ss}}\hat{a}^\dagger - \hat{a}^\dagger\hat{a}\hat{\rho}_{\text{ss}} - \hat{\rho}_{\text{ss}}\hat{a}^\dagger\hat{a}), \quad (7)$$

where γ denotes the damping constant, $\bar{n}_{\text{th}} = \{\exp[\hbar\omega/(k_B T)] - 1\}^{-1}$ is the mean number of thermal photons, k_B is the Boltzmann constant, and T is the reservoir temperature at thermal equilibrium. The master equation can be given in terms of a Liouvillian superoperator and the steady-state solution $\hat{\rho}(t)$ can be obtained by applying, e.g., the inverse power method [30].

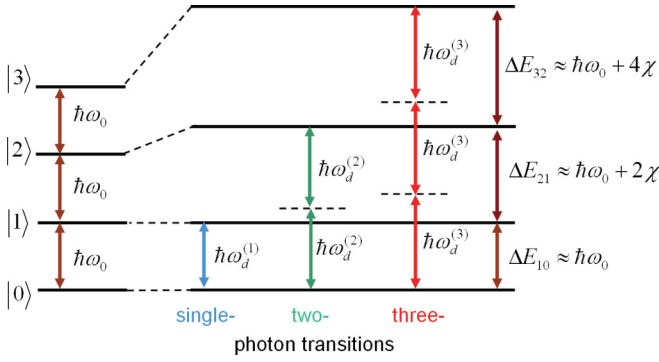


FIG. 1. (Color online) Schematic energy-level diagram explaining the occurrence of the k -photon blockade (and the k -photon-induced tunneling) in terms of the k -photon transitions induced by the driving field satisfying the resonance condition $\Delta_k = 0$, which corresponds to the driving-field frequency $\omega_d = \omega_d^{(k)} = \omega_0 + \chi(k-1)$. Due to the Kerr-type nonlinearity (induced by, e.g., a qubit), the cavity-mode levels $E_n^{(0)} = n\hbar\omega_0$ (shown on the left) become nonequidistant as $\Delta E_{n+1,n} = E_{n+1} - E_n \neq \text{const}$, where $E_n \approx n[\hbar\omega_0 + (n-1)\chi]$ (for $n = 0, 1, \dots$) are the eigenvalues of the Hamiltonian \hat{H} , given by Eq. (1), assuming $\epsilon \ll \chi$.

The single-PB can occur if the conditions

$$\gamma \ll \epsilon \ll \chi \quad (8)$$

are satisfied. Hereafter, we only analyze the resonant case $\Delta_k = 0$, which is related to the resonant k -photon transitions shown in Fig. 1. This condition implies that the tuning parameter k is related to the Kerr nonlinearity and the driving-field and cavity frequencies as follows:

$$k = (\omega_d - \omega_0)/\chi + 1. \quad (9)$$

Figure 2 shows how the photon-number probabilities P_n of the steady states depend on the tuning parameter k . By analyzing this figure, one can discover various kinds of PB effects, which appear not only for the standard resonant case of $k = 1$ but also for $k \neq 1$. For example, in the special case of $k = 2$, a higher-order effect occurs with at most two photons effectively generated in the system. We refer to this effect as the *two-photon blockade*, which means that the single- and two-photon Fock states blockade the generation of more photons.

Figure 2(b), which is similar to Fig. 2(a) but obtained assuming larger driving strength ϵ , clearly shows a *three-photon blockade* for $k = 3$, which refers to a phenomenon where the Fock states $|m\rangle$ (for $m = 1, 2, 3$) blockade the transmission of the Fock states $|n\rangle$ with higher photon number (i.e., $n > 3$). Note that, in Fig. 2(a) for $k = 3$, the probabilities of generating $|1\rangle$, $|2\rangle$, and $|3\rangle$ are nonzero but are much lower than the probability of observing the vacuum state. So, this behavior for the parameters of Fig. 2(a), contrary to Fig. 2(b), cannot be considered a genuine three-PB.

It is also quite evident why it is necessary to increase the strength of the driving field to obtain a good-quality three-PB since we need a larger average photon number. For weak driving, the average photon number of the driving field is less than three photons, thus this is not enough to induce a three-photon transition as shown in Fig. 1.

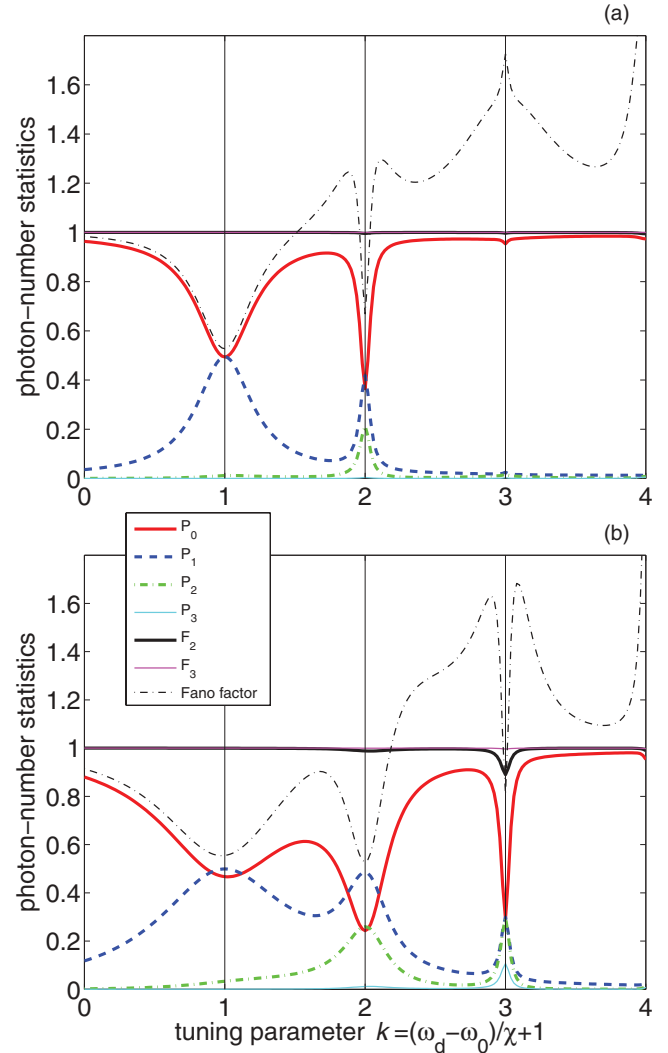


FIG. 2. (Color online) Photon-number probabilities $P_n = \langle n | \hat{\rho}_{ss} | n \rangle$ for the steady-state solutions $\hat{\rho}_{ss}$ of the master equation for the Hamiltonian $\hat{H}_{\text{rot}}^{(k)}(0)$ as a function of the tuning parameter k assuming the driving strengths (a) $\epsilon = 5\gamma$ and (b) $\epsilon = 11.56\gamma$. Moreover, we assume the Kerr nonlinearity $\chi = 30\gamma$, the damping constant $\gamma = 1$, and the mean number of thermal photons $\bar{n}_{\text{th}} = 0.01$. Figures also show the truncation fidelity F_m (for $m = 2, 3$) and the Fano factor F . Note that the field exhibits sub-Poisson (super-Poisson) photon-number statistics if $F < 1$ ($F > 1$). It is seen in both figures that resonances at $k = 1$ and 2 can be interpreted as the single- and two-photon blockades, respectively. But the three-photon blockade at $k = 3$ is apparent in (b) only.

In Fig. 2, in particular, we show the fidelity of the m -photon truncation defined as

$$F_m(\hat{\rho}_{ss}) = \sum_{n=0}^m P_n = \sum_{n=0}^m \langle n | \hat{\rho}_{ss} | n \rangle. \quad (10)$$

We refer to the m -PB if the truncation fidelity $F_m \approx 1$ and $F_n \ll 1$ for $n < m$. In Fig. 2(a), it is seen that $F_1 \approx 1$ at $k = 1$ ($F_2 \approx 1$ at $k = 2$) corresponding to the single-PB (two-PB). But the resonance at $k = 3$, for the chosen driving strength, can hardly be considered the three-PB for the driving strength $\epsilon = 5\gamma$. By contrast, $F_3 \approx 1$ at $k = 3$ for the much higher

driving strength ($\epsilon = 11.56\gamma$), as shown in Fig. 2(b). Thus, we interpret the latter case as the true three-PB, as already mentioned.

By analyzing the dependence of the photon-number probabilities $P_n = \langle n | \hat{\rho}_{ss} | n \rangle$ on the tuning parameter k , as shown in Fig. 2(a), we observe that there is a clear dip in the vacuum-state probability P_0 and a peak in the single-photon probability P_1 at $k = 1$ and 2. The two-photon probability P_2 is nonzero only near $k = 2$. The peak maximum in P_2 does not occur at $k = 1$ but it is evident at $k = 2$, which implies that the single-photon truncation fidelity F_1 differs from 1 near $k = 2$. By contrast, the two-photon truncation fidelity F_2 on the scale of Fig. 2(a) is practically equal to one. Thus, the contribution of Fock's states with three or more photons is negligible. For these reasons, we refer to the two-PB at $k = 2$. One can see in Fig. 2(a) a very slight dip in P_0 at $k = 3$, which can be, however, much deeper for the approximately twice-larger driving strength ϵ , as shown in Fig. 2(b). The dip in P_0 at $k = 3$ is accompanied by the clear appearance of the peaks of P_n for the photon numbers $n = 1, 2, 3$. It is seen that for $k = 3$ (but also close to this point), the three-photon truncation fidelity $F_3 \approx 1$ contrary to $F_2 \ll 1$. This explains why we refer to this effect as the three-PB at $k = 3$ for a suitably large driving strength ϵ as, e.g., in Fig. 2(b).

Figure 3 shows how by increasing the driving strength ϵ one can change the steady-state probabilities of the generation of n photons for chosen values of the Kerr nonlinearity, damping constant, and for the resonance conditions (a) $k = 2$ and (b) $k = 3$. We also depicted the two- and three-photon truncation fidelities, which practically equal to 1 for all the values of ϵ in Figs. 3(a) and 3(b), respectively. It is seen that for the small driving strength one cannot generate photons in the cavity in the steady-state limit, as $P_0 \approx 1$. This is a trivial case, which can be interpreted as the zero-PB. For larger values of ϵ , the true single- and two-PB effects are observed. In particular, it is seen in Fig. 3(b) that for the driving strength $\epsilon = 11.56$ the probabilities P_n of observing $n = 0, 1, 2$ photons are approximately the same. The three-photon

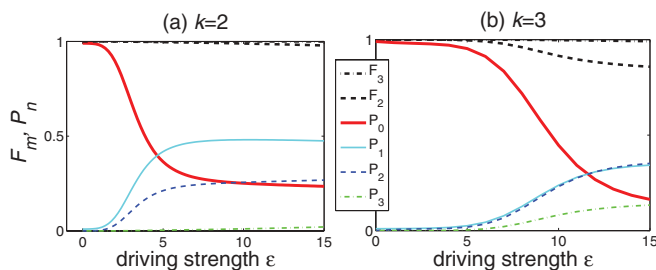


FIG. 3. (Color online) Photon-number probabilities $P_n = \langle n | \hat{\rho}_{ss} | n \rangle$ and fidelities $F_m = \sum_{n=0}^m P_n$ of the m -photon truncation for the Hamiltonian $\hat{H}_{\text{rot}}^{(k)}(0)$ for the resonances at (a) $k = 2$ and (b) $k = 3$ as a function of the driving strength ϵ assuming the Kerr nonlinearity $\chi = 30\gamma$, the damping constant $\gamma = 1$, and the mean thermal-photon number $\bar{n}_{\text{th}} = 0.01$. Note that $P_0 \approx P_1 \approx P_2$ for the driving strength $\epsilon = 11.56$ and $k = 3$. This value of ϵ is chosen in Figs. 2(b), 5, and 8 (for $k = 3$), and 11. Also note that in (a) for $k = 2$, there are two crossings, one for $P_0 = P_1$ and another one for $P_0 = P_2$.

probability is smaller but still nonzero. We have chosen this ϵ to analyze various properties of the three-PB in Fig. 2 and other figures.

III. ANALYTICAL DESCRIPTION OF PHOTON BLOCKADES

A. Steady-state photon blockade

Here, we explain analytically the standard (i.e., steady-state) PB effects, i.e., by including dissipation in the system in the infinite-time limit.

We start from the infinite-dimensional Hamiltonian, given by Eq. (5) in the resonant case $\Delta_k = 0$ for a given k , and formally truncate it to a finite-dimensional Hilbert space. For example, to show explicitly the two-PB ($k = 2$), one should analyze the Hamiltonian at least in the four-dimensional Hilbert space:

$$\hat{H}_{\text{trunc}}^{(2)}(0) = \begin{pmatrix} 0 & \epsilon & 0 & 0 \\ \epsilon & -\chi & \sqrt{2}\epsilon & 0 \\ 0 & \sqrt{2}\epsilon & 0 & \sqrt{3}\epsilon \\ 0 & 0 & \sqrt{3}\epsilon & 3\chi \end{pmatrix}, \quad (11)$$

which is given in the standard Fock basis. We have to show that the contribution of three-photon terms ($\langle 3 | \hat{\rho}_{ss}^{(2)} | n \rangle$) in the steady-state density matrix is negligible.

The conditions given by Eq. (8) should be fulfilled to observe a PB effect, so let us denote

$$\frac{\gamma}{\epsilon} = \delta, \quad \frac{\epsilon}{\chi} = d\delta, \quad (12)$$

where $\delta \ll 1$ and $d\delta \ll 1$. To find an analytical approximate steady-state solution for $\hat{\rho}_{ss}^{(2)}$, we substitute the truncated four-dimensional Hamiltonian into the master equation, given by Eq. (7), and solve the set of equations for each of the Fock-state elements of the density matrix $\langle m | \hat{\rho}_{ss}^{(2)} | n \rangle$, for $m, n = 0, 1, 2, 3$. Then we expand these solutions in power series of δ and neglect terms proportional to δ^2 or higher powers. Thus, we find the following approximate steady-state solution up to δ^1 :

$$\hat{\rho}_{ss}^{(2)} \approx \frac{1}{1 + 8d^2} \begin{pmatrix} 1 + 2d^2 & x^*\delta & id\sqrt{2} & z^*\delta \\ x\delta & 4d^2 & y^*\delta & 0 \\ -id\sqrt{2} & y\delta & 2d^2 & -\frac{2}{3}\sqrt{3}d^3\delta \\ z\delta & 0 & -\frac{2}{3}\sqrt{3}d^3\delta & 0 \end{pmatrix}, \quad (13)$$

where $x = -2d^3 - 2id^2 + d$, $y = -\sqrt{2}d^2(2d + i)$, and $z = \frac{1}{3}i\sqrt{6}d^2$. Our numerical solutions slightly differ from Eq. (13) for the parameters chosen in Fig. 2(a), but it is clearly seen that the contribution of the three-photon terms ($\langle 3 | \hat{\rho}_{ss}^{(2)} | 3 \rangle$) can be neglected, contrary to the terms $\langle m | \hat{\rho}_{ss}^{(2)} | m \rangle$ with smaller number m of photons. Also other elements ($\langle 3 | \hat{\rho}_{ss}^{(2)} | m \rangle$) are either equal to zero (for $m = 1$) or proportional to $\delta \ll 1$ (for $m = 0, 2$), so they can be neglected. Thus, our solutions explain the two-PB.

For comparison, let us analyze the single-PB described by the infinite-dimensional Hamiltonians, given by Eqs. (4) or (5) for $k = 1$, but truncated to the three-dimensional subspace, as

given by

$$\hat{H}_{\text{trunc}}^{(1)}(0) = \begin{pmatrix} 0 & \epsilon & 0 \\ \epsilon & 0 & \sqrt{2}\epsilon \\ 0 & \sqrt{2}\epsilon & 2\chi \end{pmatrix}. \quad (14)$$

By performing calculations analogous to the former case, we find the following steady-state solution up to δ^2 :

$$\hat{\rho}_{\text{ss}}^{(1)} \approx \begin{pmatrix} \frac{1}{2} + \frac{1}{16}(1 - 4d^2)\delta^2 & x^*\delta & y^*\delta^2 \\ x\delta & \frac{1}{2} - \frac{1}{16}\delta^2 & -\frac{1}{4}\sqrt{2}d\delta \\ y\delta^2 & -\frac{1}{4}\sqrt{2}d\delta & \frac{1}{4}d^2\delta^2 \end{pmatrix}, \quad (15)$$

where $x = -\frac{1}{4}(2d + i)$ and $y = \frac{1}{8}\sqrt{2}d(d + i)$, which reduces to

$$\hat{\rho}_{\text{ss}}^{(1)} \approx \frac{1}{2} \begin{pmatrix} 1 & -(d - \frac{1}{2}i)\delta & 0 \\ -(d + \frac{1}{2}i)\delta & 1 & -\frac{1}{2}d\sqrt{2}\delta \\ 0 & -\frac{1}{2}d\sqrt{2}\delta & 0 \end{pmatrix} \quad (16)$$

assuming $\delta^2 \approx 0$. It is seen in Eq. (16) that $\langle 2|\hat{\rho}_{\text{ss}}^{(1)}|n \rangle$ vanishes for $n = 0, 2$ and is $\sim \delta \ll 1$ for $n = 1$. So, the contribution of all the two-photon states can be neglected, which clearly explains the physical meaning of the single-PB for $k = 1$. Note that $\langle 2|\hat{\rho}_{\text{ss}}^{(2)}|2 \rangle \neq 0$ as described by Eq. (13), which corresponds to the two-PB for $k = 2$.

B. Photon blockade without dissipation

Here, we shortly describe nonstationary-state PB assuming no dissipation. The main results of this section are summarized in Figs. 4 and 5.

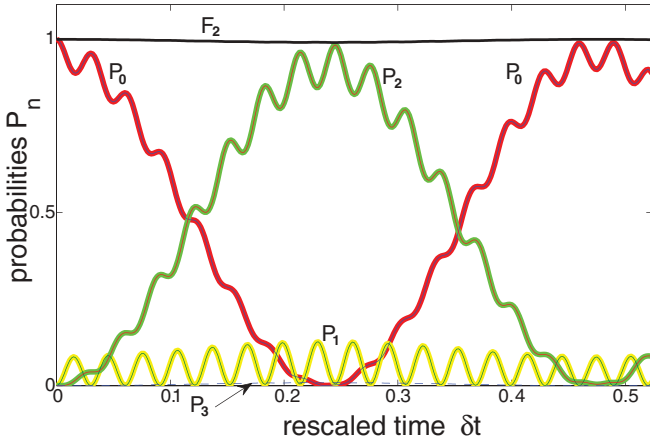


FIG. 4. (Color online) Two-photon blockade without dissipation: Evolution of the photon-number probabilities P_n for the tuning parameter $k = 2$ according to our precise numerical calculations (thin curves) in the 100-dimensional Hilbert space and approximate solutions (thick curves), given by Eqs. (17)–(22), obtained in the truncated four-dimensional Hilbert space. Excellent agreement of these solutions implies that the truncation fidelity $F_2 = P_0 + P_1 + P_2$ is almost exactly equal to one (as shown by the black line). This explains the meaning of the optical-state truncation or the nonstationary-state two-photon blockade. It is seen that the main contribution to F_2 is from the Fock states $|0\rangle$ and $|2\rangle$, which corresponds to the two-photon transitions shown in Fig. 1.

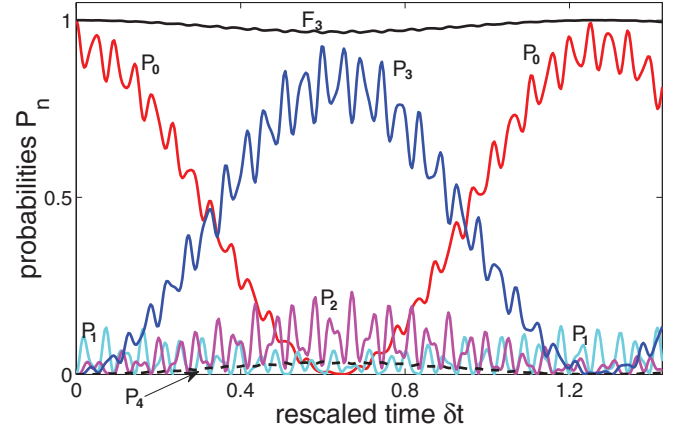


FIG. 5. (Color online) Three-photon blockade without dissipation: Evolution of the photon-number probabilities P_n as in Fig. 4 but for $k = 3$ and all the parameters (except $\gamma = 0$) as in Fig. 2(b). It is seen that the three-photon truncation fidelity F_3 slightly deviates from one. For clarity, we present here only precise solutions obtained in a large-dimensional Hilbert space. It is evident that solely the Fock states $|0\rangle$ and $|3\rangle$ are interchangeably highly populated, which corresponds to the three-photon transitions shown in Fig. 1. The probabilities P_n for $n = 1, 2$ are relatively small but not negligible, while P_n for $n > 3$ can practically be ignored (e.g., P_4 is shown by the broken curve).

To describe the two-PB, let us formally confine the Hilbert space of our system to four dimensions. Thus, we use the Hamiltonian, given by Eq. (11). Its exact eigenvalues and eigenvectors can be calculated analytically, but they are too lengthy to be presented here. Instead of this, we define a small parameter $\delta \ll 1$ as the ratio of the driving strength ϵ and the Kerr nonlinearity χ as given in Eq. (12) but, for simplicity, we assume here $d = 1$. Then, we find the power-series expansion in δ and keep the terms up to δ^2 only. Thus, we find the following eigenvalues:

$$\begin{aligned} \lambda_1 &\approx -\chi(3\delta^2 + 1), & \lambda_2 &\approx \chi\delta^2 x_-, \\ \lambda_3 &\approx \chi\delta^2 x_+, & \lambda_4 &\approx \chi(\delta^2 + 3), \end{aligned} \quad (17)$$

and the corresponding eigenvectors:

$$|\lambda_1\rangle \approx N_1[2\sqrt{2}\delta|0\rangle - 2\sqrt{2}(3\delta^2 + 1)|1\rangle + 4\delta|2\rangle - \sqrt{3}\delta^2|3\rangle], \quad (18)$$

$$|\lambda_2\rangle \approx N_-[(\delta^2 + 3)|0\rangle + 3x_- \delta|1\rangle + (x_- \delta^2 - 3)|2\rangle + \sqrt{3}\delta|3\rangle], \quad (19)$$

$$|\lambda_3\rangle \approx N_+[(\delta^2 + 3)|0\rangle + 3x_+ \delta|1\rangle - (x_+ \delta^2 - 3)|2\rangle - \sqrt{3}\delta|3\rangle], \quad (20)$$

$$|\lambda_4\rangle \approx N_4[\delta^2|1\rangle + 2\sqrt{2}\delta|2\rangle + 2\sqrt{6}|3\rangle], \quad (21)$$

where $x_{\pm} = 1 \pm \sqrt{2}$, and the normalization constants are $N_1^{-2} \approx 8(1 + 9\delta^2)$, $N_{\pm}^{-2} \approx 6(3 + 5 \pm 2\sqrt{2}\delta^2)$, and $N_4^{-2} \approx 8(3 + \delta^2)$. So, assuming no damping and no photons initially in the cavity, the time evolution of the truncated system can be

given by

$$|\psi(t)\rangle = \sum_{j=1}^3 \exp(-i\lambda_j t) \langle \lambda_j | 0 \rangle |\lambda_j\rangle + O(\delta^3). \quad (22)$$

Note that, since the initial state is $|0\rangle$, there is no contribution of $|\lambda_4\rangle$. After substituting Eqs. (17)–(21) into Eq. (22), we find that

$$\begin{aligned} \langle 3 | \psi(t) \rangle &= \frac{\sqrt{6}}{2} \delta (e^{-i\lambda_2 t} - e^{-i\lambda_3 t}) + O(\delta^3) \\ &= \frac{\delta^3}{\sqrt{3}} (2 - 3e^{it} + i6t) + O(\delta^3) = O(\delta^3), \end{aligned} \quad (23)$$

which shows explicitly the negligible contribution from the three-photon Fock state in the generated state $|\psi(t)\rangle$. Analogously we can show no important contribution from the Fock states with more photons. Thus, we conclude the occurrence of two-PB in the dissipation-free system.

In Fig. 4, we compare (i) the analytical approximate solution, given by Eq. (22), with numerical solutions obtained in the Hilbert spaces of dimension (ii) $N_{\text{dim}} = 100$ (which effectively corresponds to $N_{\text{dim}} = \infty$) and (iii) $N_{\text{dim}} = 4$ (without applying expansions in the power series of δ) for some parameters satisfying the conditions (8). On the scale of Fig. 4, there is apparently no difference between the solutions (ii) and (iii) at all, and very tiny discrepancy between them and the analytical approximate solution (i) for the relatively large $\delta = 1/6$. This excellent agreement between the approximate and precise solutions, convincingly demonstrate the blockade up to the two-photon state $|2\rangle$. It is worth stressing that, although the contribution of the three-photon state $|3\rangle$ is very small, the calculations have to be performed in the Hilbert space including the state $|3\rangle$.

For comparison, we recall that the truncated three-dimensional Hamiltonian $\hat{H}_{\text{trunc}}^{(1)}(0)$ under standard conditions, given by Eq. (8), leads to the following simple evolution:

$$|\psi(t)\rangle = \cos(\epsilon t) |0\rangle - i \sin(\epsilon t) |1\rangle + O(\delta^2), \quad (24)$$

assuming $|\psi(0)\rangle = |0\rangle$. As shown by Leoński and Tanaś in Ref. [3], this solution well approximates the precise numerical evolution of the infinite-dimensional system. This effect we refer to as the nonstationary-state single-PB, but it is usually called the single-photon optical truncation [4].

Finally, we note that these PB effects can also be interpreted as *photon-induced tunneling* studied in the context of PB in, e.g., Refs. [11,16,31]. An especially simple interpretation can be found for the dissipation-free PBs. Specifically, we can say that the PB effect for $k = 2$, as shown in Fig. 4, mainly corresponds to the *dominant* transition from the ground to the second-excited state with the two-photon resonant transition condition as schematically presented in Fig. 1. Analogously, the PB effect for $k = 3$, as shown in Fig. 5, describes mainly the three-photon resonant transition from the ground to the third-excited state, which can be explained with the help of Fig. 1. Due to amplitude dissipation, the population of lower-excited states increases, as seen by comparing Figs. 2(a) and 4 for the two-PB, as well as Figs. 2(b) and 5 for the three-PB.

IV. QUANTUM SIGNATURES OF PHOTON BLOCKADES

A. Photon-number signatures of photon blockades

We have already discussed some photon-number signatures of the PB effects by analyzing Fig. 2. Now, we focus on demonstrating the nonclassicality of the generated steady states. We recall that the nonclassicality (or quantumness) of a bosonic system is usually understood if the system is described by a nonpositive Glauber-Sudarshan quasiprobability function [32] or, equivalently, by a negative normally ordered matrix of moments [33,34]. In particular, the nonclassicality can often be revealed by analyzing photon-number properties only.

Thus, in Fig. 2, we plotted the Fano factor, which is defined by [32]

$$F(\hat{\rho}_{\text{ss}}) = \frac{\langle \hat{n}^2 \rangle - \langle \hat{n} \rangle^2}{\langle \hat{n} \rangle}. \quad (25)$$

A given state exhibits sub-Poisson (super-Poisson) photon-number statistics if $F < 1$ ($F > 1$). The sub-Poisson statistics is a nonclassical effect.

It is seen that the generated state exhibits the sub-Poisson photon-number statistics for $k < 1.5$ and near $k = 2$ as described by the Fano factors for the parameters chosen in Fig. 2(a). Global and local minima of the sub-Poisson statistics occur for the single-PB ($k = 1$) and two-PB ($k = 2$), respectively. Note the occurrence of local maxima of the Fano factors at points relatively close to $k = 2$. There are also local maxima at $k = 3$ and 4 for the parameters ϵ , χ , and γ chosen in Fig. 2(a). However, for the approximately twice-larger driving strength ϵ as in, e.g., Fig. 2(b), we can also observe at $k = 3$ a local minimum below 1 of the Fano factor, which corresponds to the sub-Poisson statistics of the three-PB.

B. Coherence and entropic signatures of photon blockades

In order to show how the steady-state solutions $\hat{\rho}_{\text{ss}}$ depend on the tuning parameter k , we also analyze their coherence properties.

Off-diagonal elements $\rho_{nm} = \langle n | \hat{\rho}_{\text{ss}} | m \rangle$ (for $n \neq m$) of the density matrix $\hat{\rho}_{\text{ss}}$, which are also often called coherences, are shown in Fig. 6. It is seen that almost all plotted coherences

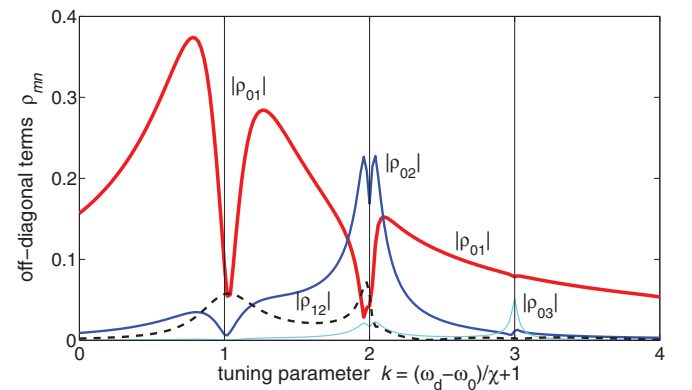


FIG. 6. (Color online) Off-diagonal elements $\rho_{nm} = \langle n | \hat{\rho}_{\text{ss}} | m \rangle$ of the steady states $\hat{\rho}_{\text{ss}}$ as a function of the tuning parameter k for the same parameters as in Fig. 2(a). These nonzero coherences demonstrate that the steady states are not maximally mixed even when k is not an integer.

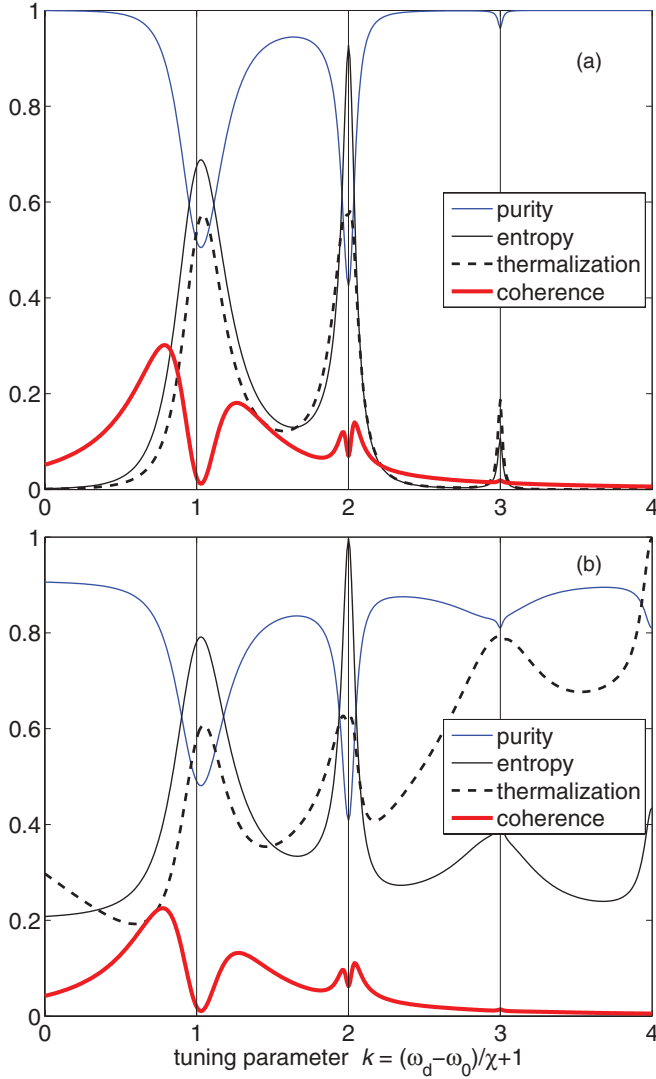


FIG. 7. (Color online) The purity $\mu(\hat{\rho}_{ss})$, von Neumann entropy $S(\hat{\rho}_{ss})$, thermalization $T_{\text{therm}}(\hat{\rho}_{ss})$, and coherence $C(\hat{\rho}_{ss})$ as a function of the tuning parameter k for the mean thermal-photon numbers (a) $\bar{n}_{\text{th}} = 0$ and (b) $\bar{n}_{\text{th}} = 0.05$ with other parameters chosen the same as in Fig. 2(a). This figure shows how thermal photons strongly affect μ , S , and T_{therm} , but do not much affect C .

do not vanish in the steady states even for off resonances (i.e., when the tuning parameter k is not an integer). This means that the generated steady states are not completely mixed.

Our deeper analysis of the coherence properties of the steady states presented in Fig. 7 includes the following measures: the purity $\mu(\hat{\rho}_{ss}) = \text{tr}(\hat{\rho}_{ss}^2)$ and the coherence parameter $C(\hat{\rho}_{ss})$ defined as the sum of all off-diagonal terms of the density matrix $\hat{\rho}_{ss}$ (see, e.g., [35]):

$$C(\hat{\rho}_{ss}) = \sum_{n \neq m} |\rho_{nm}|^2 = \text{tr}[(\hat{\rho}_{ss} - \hat{\rho}_{\text{diag}})^2] = \mu(\hat{\rho}_{ss}) - \mu(\hat{\rho}_{\text{diag}}), \quad (26)$$

where $\hat{\rho}_{\text{diag}} = \sum_n \rho_{nn} |n\rangle\langle n|$. Thus, this parameter is just the total-state purity after subtracting the diagonal-state purity. It is worth noting that C is sometimes additionally normalized [35].

It is seen that decoherence, understood as the vanishing of the off-diagonal elements of a density matrix, can intuitively be quantified by $C(\hat{\rho}_{ss})$.

To describe the mixedness of the generated steady state, we calculate the von Neumann entropy $S(\hat{\rho}_{ss}) = -\text{tr}(\hat{\rho}_{ss} \ln \hat{\rho}_{ss})$ and the thermalization parameter defined for a finite-dimensional system as [35]

$$T(\hat{\rho}_{ss}) = \frac{S_L(\hat{\rho}_{ss})}{\sqrt{\text{tr}[(\hat{\rho} - \hat{\rho}_0)^2] \text{tr}[(\hat{\rho} - \hat{\rho}_{\text{max}})^2]}} = \frac{S_L(\hat{\rho}_{ss})}{\sqrt{[1 + \mu(\hat{\rho}_{ss}) - 2p_0][1 + \mu(\hat{\rho}_{ss}) - 2p_{\text{max}}]}}, \quad (27)$$

which is defined as a properly normalized linear entropy $S_L(\hat{\rho}_{ss})$. Here, $\hat{\rho}_0 = |0\rangle\langle 0|$, $\hat{\rho}_{\text{max}} = |n_{\text{max}}\rangle\langle n_{\text{max}}|$, $p_0 = \langle 0|\hat{\rho}_{ss}|0\rangle$, $p_{\text{max}} = \langle n_{\text{max}}|\hat{\rho}_{ss}|n_{\text{max}}\rangle$, and $|n_{\text{max}}\rangle$ is the uppermost Fock state generated in the system. As explained in Ref. [35], this normalization of the linear entropy is done to exclude somehow the contribution of the ground state $\hat{\rho}_0 = |0\rangle\langle 0|$, which has a double nature: It is both a pure state and a completely decoherent equilibrium state (as in our model without the driving force). Moreover, the linear entropy $S_L(\hat{\rho}_{ss})$, which is another parameter of mixedness, can easily be obtained from the purity (depicted in Fig. 7), since $S_L(\hat{\rho}_{ss}) = 1 - \mu(\hat{\rho}_{ss})$. Other aspects of the quantum entropies and mixedness in the discussed model (but only in the special case of $k = 1$) were studied in Ref. [36].

One can clearly see in Fig. 7 that the entropy $S(\hat{\rho}_{ss})$ and thermalization $T_{\text{therm}}(\hat{\rho}_{ss})$ reach maxima and, equivalently, the purity $\mu(\hat{\rho}_{ss})$ and coherence $C(\hat{\rho}_{ss})$ parameters have minima at (or very close to) $k = 1, 2, 3$. It is worth comparing this behavior with the Fano factor $F(\hat{\rho}_{ss})$ shown in Fig. 2(a) for the same parameters, where maxima are observed only for $k = 1$ and 2 (where the PBs are predicted), while for $k = 3$ the minimum occurs, which corresponds to the case where the PB is practically not observed for the chosen parameters, as we conclude by analyzing the probabilities P_n shown in Fig. 2(a). By contrast, the coherence parameter $C(\hat{\rho})$ has minima at $k \approx 1, 2$ and very small maximum at $k = 3$. By comparing Figs. 7(a) and 7(b) obtained for the system coupled to a zero- and nonzero-temperature reservoir, we can easily see how the PBs are sensitive to temperature or, equivalently, to the number \bar{n}_{th} of thermal photons. Even by adding a very small number of thermal photons, such as $\bar{n}_{\text{th}} = 0.05$, the linear and von Neumann entropies together with the thermalization parameter are noticeably increased. This is not the case for the coherence parameter $C(\hat{\rho}_{ss})$.

C. Phase-space description of photon blockades

The dynamics of quantum systems can equivalently be described by using the phase-space formalism of Wigner functions. This formalism is particularly useful for distinguishing different PB effects as we show below. The Wigner function can be defined as [37]

$$W(\alpha) = \frac{2}{\pi} \text{tr}[\hat{D}^{-1}(\alpha)\hat{\rho}\hat{D}(\alpha)\hat{P}], \quad (28)$$

where $\hat{D}(\alpha) = \exp(\alpha\hat{a}^\dagger - \alpha^*\hat{a})$ is the displacement operator with a complex number α , and $\hat{P} = \exp(i\pi\hat{a}^\dagger\hat{a})$ is the parity operator, so its action on Fock states is simply given by

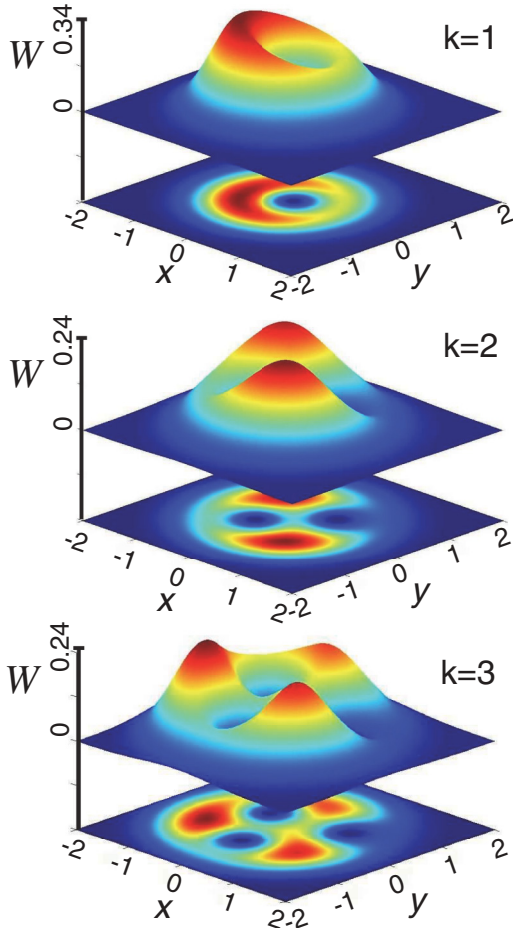


FIG. 8. (Color online) Wigner functions $W(\alpha = x + ip)$ for the k -photon blockades corresponding to the steady-state solutions of the master equation for the Hamiltonian $\hat{H}_{\text{rot}}^{(k)}(0)$, with the same parameters as in Fig. 2(a) except the driving strength $\epsilon = 11.56\gamma$ for $k = 3$. It is seen that the Wigner function for the k -photon blockade has k peaks and k dips. For $k = 3$ the peaks are deformed (due to interference in phase space) but still are visible.

$\hat{P}|n\rangle = (-1)^n|n\rangle$. The Wigner function can be generalized to the s -parametrized Cahill-Glauber quasiprobabilities [37]. Nevertheless, contrary to other definitions, Eq. (28) shows a *direct* method (i.e., without the necessity of applying quantum state tomography) to measure the Wigner function [38]. This

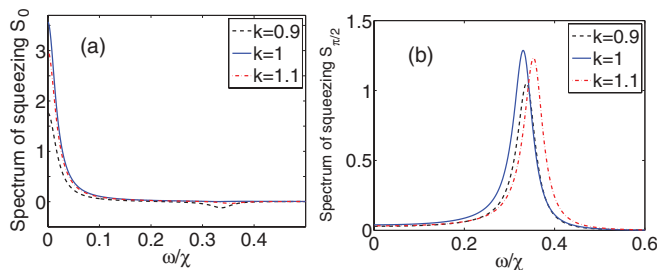


FIG. 9. (Color online) Spectra of squeezing (a) $S_0(\omega)$ and (b) $S_{\pi/2}(\omega)$ for the single-photon blockade for the same parameters as in Fig. 2(a). Broken curves show the spectra for the Hamiltonian $\hat{H}_{\text{rot}}^{(k)}(0)$ with off-resonance values of the tuning parameter k .

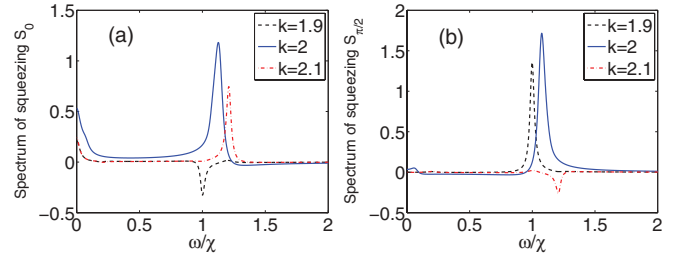


FIG. 10. (Color online) Spectra of squeezing for the two-photon blockade analogously to those in Fig. 9 but for the resonance $k = 2$ and off-resonance values of the tuning parameter k . It is seen that either S_0 or $S_{\pi/2}$ only for the off-resonant cases has a clear negative dip.

direct method was experimentally applied in, e.g., cavity QED [39] and circuit QED [40] systems.

In Fig. 8, we show the Wigner function for the blockades of up to k photons for $k = 1, 2, 3$ by properly choosing parameters in order to satisfy the resonance condition $\Delta_k = 0$ together with $\gamma \ll \epsilon \ll \chi$. The k -peak and k -dip (antipeak) structures of the Wigner functions clearly correspond to the k -PB.

D. Spectrum of squeezing for photon blockades

The PBs can also be revealed in two-time correlations. Let us analyze the two-time normally ordered ($::$) and time-ordered (T) correlation function

$$\begin{aligned} T\langle : \hat{X}_\theta(\tau) \hat{X}_\theta(0) : \rangle & \\ \equiv \lim_{t \rightarrow \infty} T\langle : \hat{X}_\theta(t + \tau) \hat{X}_\theta(t) : \rangle & \\ = \langle \hat{a}^\dagger(\tau) a(0) \rangle + \langle \hat{a}^\dagger(0) a(\tau) \rangle & \\ + e^{-2i\theta} \langle \hat{a}(\tau) a(0) \rangle + e^{2i\theta} \langle \hat{a}^\dagger(0) a^\dagger(\tau) \rangle & \end{aligned} \quad (29)$$

of the quadrature phase distribution

$$\hat{X}_\theta(t) = \hat{a}(t)e^{-i\theta} + \hat{a}^\dagger(t)e^{i\theta}. \quad (30)$$

The spectrum of squeezing is defined as the Fourier transform of the covariance [41]:

$$S_\theta(\omega) = \int_{-\infty}^{\infty} d\tau e^{-i\omega\tau} T\langle : \hat{X}_\theta(\tau) \hat{X}_\theta(0) : \rangle, \quad (31)$$

where the covariance is defined by the general formula $\langle A, B \rangle = \langle AB \rangle - \langle A \rangle \langle B \rangle$. In Figs. 9–11, we demonstrated

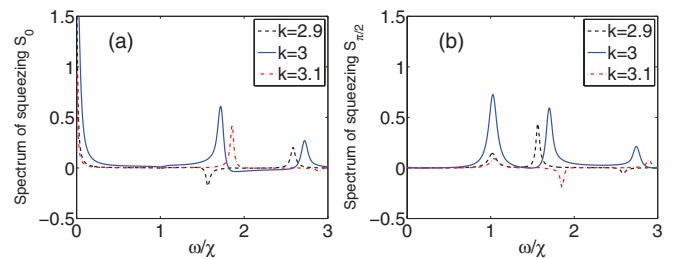


FIG. 11. (Color online) Spectra of squeezing for the three-photon blockade analogously to those in Figs. 9 and 10 but for the resonance $k = 3$ and off-resonance values of the tuning parameter k (assuming the driving strength $\epsilon = 11.56\gamma$). Analogously to the two-photon blockade, the off-resonance spectra have a negative dip either for $\theta = 0$ or $\pi/2$, which does not appear for the resonant case for $k = 3$.

distinctive properties of the spectra of squeezing for the single-PB (Fig. 9), two-PB (Fig. 10), and three-PB (Fig. 11) for the tuning parameters at the resonance, $k = k_0$, and slightly out of the resonance, $k = k_0 \pm \delta$, where $\delta \ll 1$ and $k_0 = 1, 2, 3$. Surprisingly, the spectra of squeezing as a function of the tuning parameter k are more sensitive indicators of the two- and three-PBs instead of those of the single-PB.

V. CONCLUSIONS

We studied nonlinear photon-photon interaction at the single-photon level in a system consisting of a cavity with a Kerr nonlinearity driven by a weak classical field. This is a standard prototype model, where the Kerr-like nonlinearity can be induced by the interaction of, e.g., a qubit with a cavity field in the dispersive regime.

By finding the master-equation solutions of the model in the steady-state limit for a properly chosen frequency of the classical driving field, we observed a blockade of more than one photon. This is a generalization of the single-PB for the multiphoton (say m -photon) case, which means that the Fock states with $n = 0, 1, \dots, m$ photons are, practically, the *only* generated in this nonlinear cavity. This effect can also be interpreted as the multiphoton-state truncation realized by nonlinear quantum scissors or multiphoton-induced tunneling corresponding to multiphoton transitions as schematically shown in Fig. 1.

It is worth noting that some generalizations of the single-photon nonlinear truncation processes for the multiphoton cases were already discussed by, e.g., Leoński *et al.* (see Ref. [4] for a review). Nevertheless, all these proposals assume either higher-order driving processes, as described in Ref. [21] by the Hamiltonian $H_{\text{drive}}^{(l)} = \epsilon^{(l)}[\hat{a}^l + (\hat{a}^\dagger)^l]$, or higher-order Kerr nonlinearity, corresponding to the Hamiltonian $H_{\text{Kerr}}^{(k)} = \chi^{(k+1)}(\hat{a}^\dagger)^{k+1}\hat{a}^{k+1}$ in Ref. [23], or both $\epsilon^{(k)}$ and $\chi^{(l)}$ [22] for $k, l = 2, 3, \dots$. In our approach, we assume the lowest-order parametric driving ($l = 1$) and the lowest-order Kerr nonlinearity ($k = 1$), which is the same as in the standard single-PB. Also, in the mentioned generalizations, only the free evolution was analyzed. Thus, these effects can solely be interpreted as nonstationary-field effects; so, they are almost unmeasurable. The dissipation effects were later studied, but only for the short-time evolution regime in Ref. [42]. In this paper, we focused on measurable effects, thus, we studied (except only one section) the steady-state solutions of the master equation in the infinite-time limit.

We described, as given by Eq. (9), how to choose the resonance frequency ω_d of the driving field for a given cavity frequency ω_0 and the Kerr nonlinearity χ and how to increase the driving strength ϵ (see Fig. 3) in order to observe the blockade at the multiphoton Fock state.

In our presentation we focused on the blockades of $k = 2$ and 3 photons in order to achieve high fidelity F_k of the

k -photon truncation and with a contribution of the k -photon state which cannot be neglected, which means that $F_{k-1} \ll 1$.

We showed analytically and numerically that these PBs occur both for nondissipative and dissipative systems. In particular, we showed an excellent agreement (i.e., no differences on the scale of Fig. 4) for the two-PB between the numerical solutions obtained in the Hilbert spaces of infinite dimension (practically $N_{\text{dim}} = 100$) and of finite dimension ($N_{\text{dim}} = 4$). Our approximate analytical solutions only slightly differ from the numerical ones (as shown in Fig. 4 for a relatively large δ).

We demonstrated a variety of quantum properties revealing the unique nature of the single-, two-, and three-PBs as a function of the tuning parameter k . In particular, we studied photon-number statistics (as shown in Fig. 2), as well as coherence and entropic properties (in Figs. 6 and 7). We gave a clear comparison of the Wigner functions of the steady states corresponding to the blockades of $k = 1, 2, 3$ photons (see Fig. 8). Moreover, we showed clear differences in the spectra of squeezing of the steady states in the resonant cases at $k = 1, 2, 3$ and slightly off the resonances (as shown in Figs. 9–11).

We suggested that the two-PB and three-PB can be observed in various systems, where the single-PB has already been experimentally observed [13,14,16] or, at least, theoretically predicted [17].

Analogously, a blockade of *phonons* instead of *photons* can be considered. Namely, a two-phonon generalization of the standard single-phonon blockade can be predicted in the nanomechanical systems studied in Refs. [18,19]. The crucial point is that the effective Hamiltonians, given by Eqs. (1) and (5), under proper conditions, can be obtained from other standard models in cavity QED, circuit QED, and quantum optomechanics.

The single-photon blockade has attracted considerable interest, with potential applications in quantum state engineering, quantum information, and quantum communication. We believe that the multiphoton blockades described in this paper can also find some useful quantum applications and in addition, at a fundamental level, they can show a deeper analogy between condensed-matter and optical phenomena.

ACKNOWLEDGMENTS

We thank Karol Bartkiewicz for discussions. A.M. and M.P. acknowledge the support of the Polish National Science Centre under Grants No. DEC-2011/03/B/ST2/01903 and No. DEC-2012/04/M/ST2/00789. Y.X.L. was supported by the National Natural Science Foundation of China under Grants No. 10975080 and No. 61025022. J.B. was supported by the Czech Ministry of Education under Project No. MSM6198959213. F.N. acknowledges partial support from the Army Research Office, JSPS-RFBR Contract No. 12-02-92100, Grant-in-Aid for Scientific Research (S), MEXT Kakenhi on Quantum Cybernetics, and Funding Program for Innovative R&D on S&T (FIRST).

[1] A. Imamoglu, H. Schmidt, G. Woods, and M. Deutsch, *Phys. Rev. Lett.* **79**, 1467 (1997); P. Grangier, D. F. Walls, and K. M. Gheri, *ibid.* **81**, 2833 (1998).

[2] M. A. Kastner, *Rev. Mod. Phys.* **64**, 849 (1992).

[3] W. Leoński and R. Tanaś, *Phys. Rev. A* **49**, R20 (1994); W. Leoński, S. Dyrting, and R. Tanaś, *J. Mod. Opt.* **44**, 2105 (1997).

- [4] A. Miranowicz, W. Leoński, and N. Imoto, *Adv. Chem. Phys.* **119**, 155 (2001); W. Leoński and A. Miranowicz, *ibid.* **119**, 195 (2001).
- [5] L. Tian and H. J. Carmichael, *Phys. Rev. A* **46**, R6801 (1992).
- [6] M. J. Werner and A. Imamoğlu, *Phys. Rev. A* **61**, 011801 (1999).
- [7] R. J. Brecha, P. R. Rice, and M. Xiao, *Phys. Rev. A* **59**, 2392 (1999).
- [8] S. Rebić, S. M. Tan, A. S. Parkins, and D. F. Walls, *J. Opt. B* **1**, 490 (1999).
- [9] S. Rebić, A. S. Parkins, and S. M. Tan, *Phys. Rev. A* **65**, 063804 (2002).
- [10] J. Kim, O. Bensen, H. Kan, and Y. Yamamoto, *Nature (London)* **397**, 500 (1999).
- [11] I. I. Smolyaninov, A. V. Zayats, A. Gungor, and C. C. Davis, *Phys. Rev. Lett.* **88**, 187402 (2002).
- [12] A. J. Hoffman, S. J. Srinivasan, S. Schmidt, L. Spietz, J. Aumentado, H. E. Türeci, and A. A. Houck, *Phys. Rev. Lett.* **107**, 053602 (2011).
- [13] C. Lang *et al.*, *Phys. Rev. Lett.* **106**, 243601 (2011).
- [14] K. M. Birnbaum, A. Boca, R. Miller, A. D. Boozer, T. E. Northup, and H. J. Kimble, *Nature (London)* **436**, 87 (2005).
- [15] Editor's Summary of Ref. [14], *Nature (London)* **436**, p. XV (2005).
- [16] A. Faraon, I. Fushman, D. Englund, N. Stoltz, P. Petroff, and J. Vučković, *Nat. Phys.* **4**, 859 (2008).
- [17] P. Rabl, *Phys. Rev. Lett.* **107**, 063601 (2011); A. Nunnenkamp, K. Børkje, and S. M. Girvin, *ibid.* **107**, 063602 (2011).
- [18] Y. X. Liu, A. Miranowicz, Y. B. Gao, J. Bajer, C. P. Sun, and F. Nori, *Phys. Rev. A* **82**, 032101 (2010).
- [19] N. Didier, S. Pugnetti, Y. M. Blanter, and R. Fazio, *Phys. Rev. B* **84**, 054503 (2011).
- [20] Y. X. Liu, X. W. Xu, A. Miranowicz, and F. Nori, arXiv:1203.6419.
- [21] W. Leoński, *Phys. Rev. A* **54**, 3369 (1996).
- [22] A. Miranowicz, W. Leoński, S. Dyrting, and R. Tanaś, *Acta Phys. Slov.* **46**, 451 (1996).
- [23] W. Leoński, *Phys. Rev. A* **55**, 3874 (1997).
- [24] D. T. Pegg, L. S. Phillips, and S. M. Barnett, *Phys. Rev. Lett.* **81**, 1604 (1998).
- [25] M. Koniorczyk, Z. Kurucz, A. Gabris, and J. Janszky, *Phys. Rev. A* **62**, 013802 (2000).
- [26] A. Miranowicz, *J. Opt. B* **7**, 142 (2005).
- [27] S. K. Özdemir, A. Miranowicz, M. Koashi, and N. Imoto, *Phys. Rev. A* **64**, 063818 (2001).
- [28] M. Boissonneault, J. M. Gambetta, and A. Blais, *Phys. Rev. A* **79**, 013819 (2009).
- [29] H. Carmichael, *An Open Systems Approach to Quantum Optics* (Springer, Berlin, 1993).
- [30] S. M. Tan, *J. Opt. B* **1**, 424 (1999).
- [31] A. Majumdar, M. Bajcsy, and J. Vučković, *Phys. Rev. A* **85**, 041801(R) (2012).
- [32] W. Vogel and D. G. Welsch, *Quantum Optics* (Wiley-VCH, Weinheim, 2006).
- [33] W. Vogel, *Phys. Rev. Lett.* **100**, 013605 (2008).
- [34] A. Miranowicz, M. Bartkowiak, X. Wang, Y. X. Liu, and F. Nori, *Phys. Rev. A* **82**, 013824 (2010).
- [35] V. V. Dodonov, S. S. Mizrahi, and A. L. de Souza Silva, *J. Opt. B* **2**, 271 (2000).
- [36] J. Bajer, A. Miranowicz, and M. Andrzejewski, *J. Opt. B* **6**, 387 (2004).
- [37] K. E. Cahill and R. J. Glauber, *Phys. Rev.* **177**, 1882 (1969).
- [38] L. G. Lutterbach and L. Davidovich, *Phys. Rev. Lett.* **78**, 2547 (1997).
- [39] P. Bertet, A. Auffeves, P. Maioli, S. Osnaghi, T. Meunier, M. Brune, J. M. Raimond, and S. Haroche, *Phys. Rev. Lett.* **89**, 200402 (2002).
- [40] M. Hofheinz *et al.*, *Nature (London)* **459**, 546 (2009).
- [41] D. F. Walls and G. J. Milburn, *Quantum Optics* (Springer, Berlin, 2006).
- [42] A. Miranowicz and W. Leoński, *J. Opt. B* **6**, S43 (2004).